# Microstructure and magnetic properties of Ni$_{50}$Mn$_{37}$Sn$_{13}$ Heusler alloy ribbons

J. D. Santos,[a)] T. Sanchez, P. Alvarez, M. L. Sanchez, J. L. Sánchez Llamazares, and B. Hernando
*Departamento de Física, Facultad de Ciencias, Universidad de Oviedo, Calvo Sotelo s/n, 33007 Oviedo, Spain*

Ll. Escoda and J. J. Suñol
*Universidad de Girona, Campus de Montilivi, edifici PII, Lluís Santaló s/n, 17003 Girona, Spain*

R. Varga
*Institute of Physics, Faculty of Science, UPJS, Park Angelinum 9, 04154 Kosice, Slovakia*

The Heusler alloy Ni$_{50}$Mn$_{37}$Sn$_{13}$ was successfully produced as ribbon flakes of thickness around $7-10$ $\mu$m melt spinning. Fracture cross section micrographs in the ribbon show the formation of a microcrystalline columnarlike microstructure, with their longer axes perpendicular to the ribbon plane. Phase transition temperatures of the martensite-austenite transformation were found to be $M_S=218$ K, $M_f=207$ K, $A_S=224$ K, and $A_f=232$ K; the thermal hysteresis of the transformation is 15 K. Ferromagnetic $L2_1$ bcc austenite phase shows a Curie point of 313 K, with cell parameter $a=0.5971(5)$ nm at 298 K, transforming into a modulated $7M$ orthorhombic martensite with $a=0.6121(7)$ nm, $b=0.6058(8)$ nm, and $c=0.5660(2)$ nm, at 150 K. © *2008 American Institute of Physics*. [DOI: 10.1063/1.2832330]

Ferromagnetic shape memory alloys (FSMA) are of considerable interest because of their exceptional magnetoelastic properties.[1–3] The shape memory effect can not only be controlled by changing the temperature, as it occurs in traditional shape memory alloys, but also by varying the magnetic field up to moderate field values. The latter makes them of noteworthy interest for developing new thermal or magnetically driven actuators.[4]

Among the Heusler alloys that exhibit magnetic shape memory effect, the most extensively studied are those of the Ni-Mn-Ga system. However, to overcome some of the problems related to practical application, such as the high cost of gallium and the low martensitic transformation temperature that they usually present, the search for Ga-free alloys has been recently attempted. Martensitic transformation in ferromagnetic Heusler Ni$_{50}$Mn$_{50-x}$Sn$_x$ alloys with $10 \leqslant x \leqslant 16.5$ was first reported by Sutou *et al.*[5] Later, Krenke *et al.* studied phase transformations and magnetic and magnetocaloric properties of the Ni$_{50}$Mn$_{50-x}$Sn$_x$ alloy series with $5 \leqslant x \leqslant 25$.[6,7] Samples with $x=0.13$ and 0.15 are ferromagnetic in the martensitic state undergoing a first order martensitic-austenitic structural transition at a temperature below the respective Curie points of both phases. At room temperature, the alloy with $x=0.13$ is martensitic, and the martensite-austenite transformation occurs around room temperature. Brown *et al.*[8] and Koyama *et al.*[9] reported on the structural and magnetoelastic behaviors of the alloy Ni$_{50}$Mn$_{36}$Sn$_{14}$. This alloy exhibits a large negative magnetoresistance effect accompanied by the magnetic-field-

induced reverse transformation. Khovaylo *et al.* studied Ni$_{50+x}$Mn$_{37-x}$Sn$_{13}$ and Ni$_{50+y}$Mn$_{39-y}$Sn$_{11}$ ($x$, $y=1$, 2, and 3) alloys.[11] $M_s$ and $M_p$ show a nonmonotonic dependence on the Ni excess $x$ and $y$. Han *et al.* have investigated the magnetocaloric effect in Ni$_{50-x}$Mn$_{39-x}$Sn$_{11}$ ($x=5$, 6, and 7) near the martensitic transition.[12] They report magnetic entropy changes up to 10.4 J/kg K at 10 kOe for $x=7$. Ni-Mn-Sn system is, therefore, of prospective importance as FSMA and as promising magnetic refrigerant alloy. In all these cases, alloys were produced as bulk polycrystalline samples.

In this work we produced, as far as we know for the first time, Ni-Mn-Sn alloys by rapid solidification. This procedure offers several potential advantages for the fabrication of the shape memory materials such as avoiding the homogenization annealing step to reach a single phase alloy and the synthesis of highly textured polycrystalline samples. Moreover, ribbon shape is appropriate for direct use in practical devices.[6,7] In view of its interesting properties, we have selected the alloy Ni$_{50}$Mn$_{37}$Sn$_{13}$ and studied its microstructural and magnetic properties.

As-cast Ni$_{50}$Mn$_{37}$Sn$_{13}$ were prepared by Ar arc melting from pure elements ($>99.98\%$). The samples were melt-spun in argon environment at a linear speed of 48 ms$^{-1}$.

X-ray diffraction (XRD) analyses were performed using Cu $K\alpha$ radiation with a low-temperature device (step increment 0.05°). Microstructure and elemental composition of ribbons were examined by using a scanning electron microscope (SEM) equipped with a microanalysis system.

Magnetization measurements were performed in the temperature interval of 4.2 $-350$ K using a PPMS-14T platform with the vibrating sample magnetometer module. Zero-field cooled (ZFC), field cooled (FC), and field heated (FH)

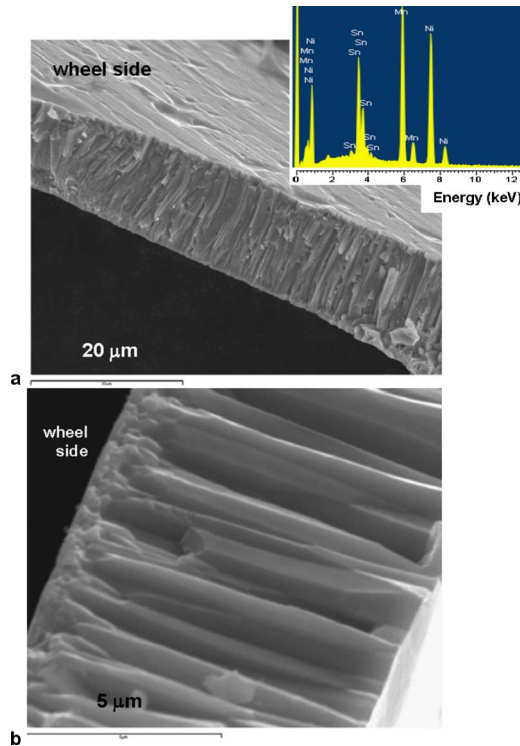a)Author to whom correspondence should be addressed. Electronic mail: jdsantos@uniovi.es.

FIG. 1. (Color online) SEM micrograph of fractured cross section of as-quenched $Ni_{50}Mn_{37}Sn_{13}$ ribbons. Inset: Typical EDS spectrum.
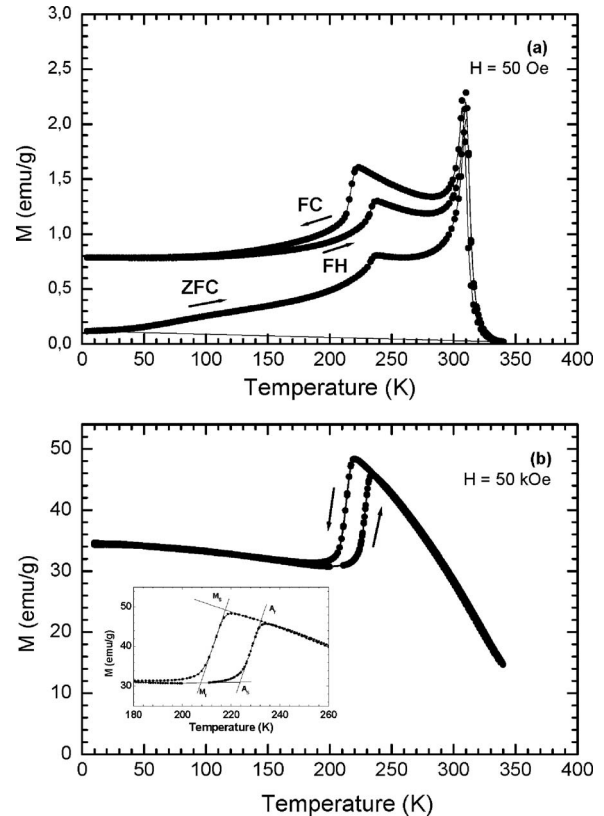


FIG. 2. Temperature dependence of magnetization measured at (a) $H$ =50 Oe and (b) $H$=50 kOe, for as-quenched $Ni_{50}Mn_{37}Sn_{13}$ ribbons. Inset of (b):heating and cooling curves where phase transition occurs.

thermomagnetic curves were recorded at $H_{ext}$=50 Oe and 50 kOe, (heating or cooling rate 2 K/min). The magnetic field was applied along the ribbon axis. Curie point $T_C$ was inferred from the minimum in the $dM/dT$ vs $T$ curve. Hysteresis loops were measured up to 10 kOe in a MPMS-5T with a superconducting quantum interference device module.

Typical SEM images at different magnifications of the facture cross section of the ribbons are shown in Fig. 1. The ribbon thickness was around 7–10 $\mu$m. As shown in Fig. 1(b), small equiaxed grains crystallize in a thin layer on the wheel side. Further, they change abruptly into an ordered columnar microstructure. The longer axis of the columnar grains tends to align perpendicularly to the ribbon plane surface, suggesting that heat removal during rapid solidification process induces directional growth of the crystalline phase formed. Grains are as large as the ribbon thickness allows.

A careful study by EDS microanalysis was carried out to estimate the average elemental chemical composition. The results show homogeneous distribution of the chemical composition (see Table I), while a typical EDS spectrum appears in the inset of Fig. 1(a). Segregation of minor or secondary phases was not observed.

TABLE I. Chemical composition determined by EDS for as-quenched $Ni_{50}Mn_{37}Sn_{13}$ ribbons.

| Location | Mn (at. %) | Ni (at. %) | Sn (at. %) |
|---|---|---|---|
| Free side | 36.53 | 50.45 | 13.02 |
| Cross section | 36.25 | 50.65 | 13.10 |
| Wheel side | 36.13 | 50.65 | 13.32 |
| Average value | 36.33 | 50.55 | 13.12 |

The ZFC, FC, and FH thermomagnetic curves recorded at 50 Oe are shown in Fig. 2(a). For ZFC curve, the magnetization increases monotonically with the temperature to have an abrupt change in the slope at $T$=236 K as a result of martensite-austenite transformation; a similar behavior is observed for the FH curve. Above the structural transformation, the magnetization shows a Hopkinson maximum. The Curie temperature for the high-temperature austenite formed is found to be $T_C$=313 K. At low fields, the splitting between the ZFC and FC curves below ferromagnetic transition $T_C$ could indicate the presence of magnetically inhomogeneous states.[7,10,11] Figure 2(b) shows the temperature dependence of saturation magnetization at 50 kOe. Contrary to the low-field measurement [Fig. 2(a)], the curve shows two well distinct ferromagnetic regions. The abrupt change in the heating and cooling $M(T)$ curves results from the reversible structural change from the low- to high-temperature martensite and austenite phases, respectively (the inset shows in detail the phase transition region). The start and finish temperatures of the martensite phase transformation are $M_S$=218 K and $M_f$=207 K, while the ones found for austenite are $A_S$ =224 K and $A_f$=232 K; the thermal hysteresis of the transformation is 15 K. It is underlined that in the ribbons produced, these characteristic temperatures are well below those reported for the bulk alloy.[6,7,13]

Hysteresis loops show ferromagnetic ordering for austenite phase at 270 K as well as for the martensite one at 150 K (see Fig. 3). Austenite phase is softer and reaches the saturation easier at low field than martensite, as a conse-
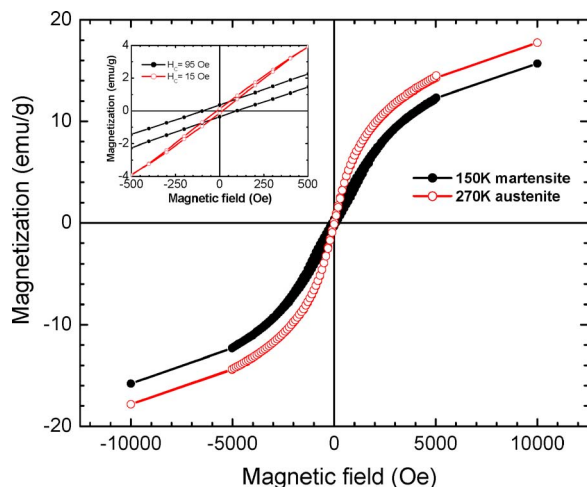
FIG. 3. (Color online) Hysteresis loops for as-quenched $Ni_{50}Mn_{37}Sn_{13}$ ribbons at 150 and 270 K. Inset: zoom into the low-field range.

quence of its lower anisotropy. The coercive field is 95 Oe for the martensite phase and 15 Oe for the austenite phase. Saturation magnetization is higher for the austenite phase as can also be seen from thermomagnetic curves [Fig. 2(b)].

X-ray diffraction patterns were recorded at 298 and 150 K. At room temperature, all Bragg peaks were well indexed on the basis of a cubic $L2_1$ structure with a lattice parameter $a = 0.5971(5)$ nm (see Fig. 4), contrary to bulk arc-melted materials where a modulated $10M$ martensite phase was found at room temperature.[6] The measurement confirms that ribbons are fully single phase with austenite as the high-
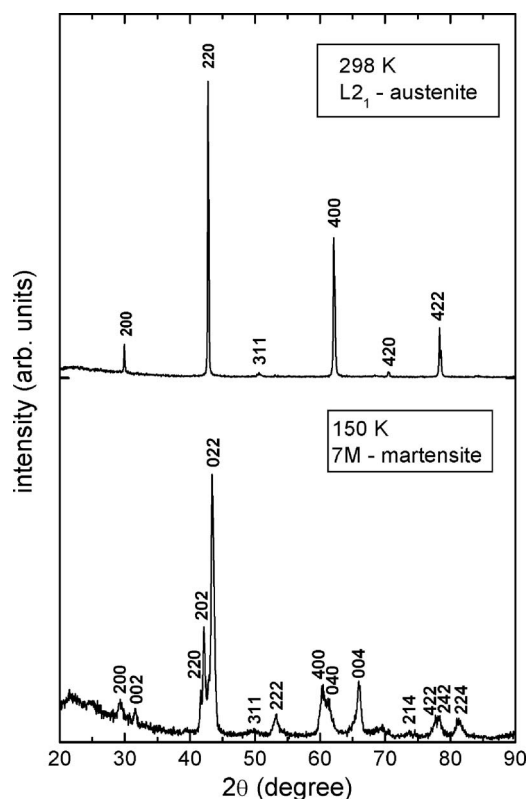
temperature phase. At a temperature below the martensitic phase transformation, the XRD pattern changes from the cubic $L2_1$ phase to an orthorhombic structure. The orthorhombic structure of the martensite formed shows a seven-layer modulation, $7M$, and the lattice parameters at 150 K are $a = 0.6121(7)$ nm, $b = 0.6058(8)$ nm, and $c = 0.0660(2)$ nm.

From a preliminary characterization of rapidly solidified $Ni_{50}Mn_{37}Sn_{13}$ ribbons by x-ray diffraction, scanning electron microscopy, and magnetization measurements, the following points can be outlined: (a) rapid solidification by melt spinning was effective in producing, in a single step, ribbons with homogeneous chemical composition and single phase cubic $L2_1$ austenite phase at room temperature; (b) ribbons exhibit a strongly ordered microstructure of columnar microcrystalline grains that grow having their longer axis aligned perpendicular to the ribbon plane; (c) at low temperature, the ferromagnetic austenite phase transforms into a seven-layered orthorhombic martensite phase. The characteristic temperatures measured for the reversible austenite-austenite phase transformation were $M_S = 218$ K, $M_f = 207$ K, $A_S = 224$ K, and $A_f = 232$ K.

The production of single phase, highly textured ribbons of this Ga-free (Ni-Mn)-based FSMA may open a new issue of considerable scientific and practical significance since a better comprehension of the factors determining the phase transformation mechanisms and the resulting magnetostructural properties is crucial for the development of technical applications.

[1] A. Sozinov, A. A. Likhachev, N. Lanska, and K. Ullakko, Appl. Phys. Lett. **80**, 1746 (2002).
[2] A. Sozinov, A. A. Likhachev, and K. Ullakko, IEEE Trans. Magn. **38**, 2814 (2002).
[3] J. Enkovaara, A. Ayuela, A. T. Zayak, P. Entel, L. Nordström, M. Dube, J. Jalkanen, J. Impola, and R. M. Nieminen, Mater. Sci. Eng., A **378**, 52 (2004).
[4] M. A. Marioni, R. O. C. O'Handley, S. M. Allen, S. R. Hall, D. I. Paul, M. L. Richard, J. Feuchtwanger, B. W. Peterson, J. M. Chambers, and R. Techapiesancahoroenkij, J. Magn. Magn. Mater. **290–291**, 35 (2005).
[5] Y. Sutuo, Y. Imano, N. Koeda, T. Omori, R. Kainuma, K. Ishida, and K. Oikawa, Appl. Phys. Lett. **85**, 4358 (2004).
[6] T. Krenke, M. Acet, E. F. Wassermann, X. Moya, L. Mañosa, and A. Planes, Phys. Rev. B **72**, 014412 (2005).
[7] T. Krenke, E. Duman, M. Acet, E. F. Wassermann, X. Moya, L. Mañosa, and A. Planes, Nat. Mater. **4**, 450 (2005).
[8] P. J. Brown, A. P. Gandy, K. Ishida, R. Kainuma, T. Kanomata, K. U. Neumann, K. Oikata, B. Ouladdiaf, and K. R. A. Ziebeck, J. Phys.: Condens. Matter **18**, 2249 (2006).
[9] K. Koyama, K. Watanabe, T. Kanomata, R. Kainuma, K. Oikawa, and K. Ishida, Appl. Phys. Lett. **88**, 132505 (2006).
[10] K. Koyama, H. Okada, K. Watanabe, T. Kanomata, R. Kainuma, W. Ito, K. Oikawa, and K. Ishida, Appl. Phys. Lett. **89**, 182510 (2006).
[11] V. Khovaylo, V. Koledov, V. Shavrov, V. Novosad, A. Korolyov, M. Ohtsuka, O. Saveel'eva, and T. Takagi, Adv. Funct. Mater. **13**, 474 (2006).
[12] Z. D. Han, D. H. Wang, C. L. Zhang, H. C. Xuan, B. X. Gu, and Y. W. Du, Appl. Phys. Lett. **90**, 042507 (2007).
[13] E. Duman, M. Acet, Y. Elerman, A. Elmali, and E. F. Wassermann, J. Magn. Magn. Mater. **238**, 11 (2002).



FIG. 4. X-ray diffraction patterns for as-quenched $Ni_{50}Mn_{37}Sn_{13}$ ribbons measured at 298 K (up) and 150 K (down).